Period Estimation for Time-Varying Graph Signals and Its Application to Graph Wiener Filter

Tsutahiro Fukuhara, Junya Hara, Hiroshi Higashi, and Yuichi Tanaka
Graduate School of Engineering, The University of Osaka, Japan
E-mail: t.fukuhara@msp-lab.org, {j.hara, higashi, ytanaka}@comm.eng.osaka-u.ac.jp

***Abstract*—This paper proposes a period estimation method for time-varying graph signals (TVGSs) and we apply it to graph Wiener filter. In many network-based measurements, TVGSs are stationary in the spatial domain and also exhibit *periodic stationarity* in the time domain. Although the accurate period estimation of TVGSs would result in accuracy gains in applications, most existing works ignore their periodic behaviors, while standard time domain signals naturally exhibit such periodicity. In this paper, we first introduce *cyclic graph wide sense stationarity*, where signals are stationary in the spatial domain and periodic stationary in the time domain. Second, we propose a period estimation method based on the assumption. It consists of two phases: 1) periodic features are extracted from TVGSs by decomposing them using graph Fourier transform and a nested periodic dictionary, and 2) a period is estimated by calculating features indicating the dominant period of the features extracted in the first phase. Thanks to the accurate period estimation and cyclic graph wide sense stationarity, we can construct a graph Wiener filter for TVGSs. Numerical experiments on real-world data demonstrate that our method effectively estimates underlying periods from data, and the proposed Wiener filter exhibits superior performance to existing methods.**

I. Introduction

In sensor networks, spatially distributed sensors collect environmental data and communicate over a network [1]. They are mathematically modeled as a graph, where sensors are represented as nodes, and communication links among sensors are represented as edges. Observed data on sensor networks can be regarded as time-varying signals on the underlying graph, referred to as time-varying graph signals (TVGSs) [2].

TVGS analysis needs to consider both spatial and temporal relationships. Existing studies on TVGSs typically assume graph wide sense stationarity (GWSS), where signals are stationary in the node domain [3]–[5]. Under this assumption, the spatial relationships can be characterized using graph spectral analysis techniques, such as graph Fourier transform (GFT) and/or graph wavelet transforms [2], [6]. However, since GWSS is inherently designed for static graph signals, the temporal relationships of TVGSs are not covered with this assumption. Some studies consider *joint* wide sense stationarity (JWSS), where signals are assumed to be stationary in the joint node-time domain [7]–[9]. However, JWSS often oversimplifies spatial and/or temporal behavior in the wild owing to its strong assumption in both domains.

This work is supported in part by JSPS KAKENHI under Grants 23K26110, 23K17461, and 24K21314, and JST AdCORP under Grant JPMJKB2307.

Many time domain signals, including TVGSs, often exhibit stationarity over periodic time intervals, as can be observed in temperature, humidity, sea level, and traffic volume [10]–[12]. This phenomenon, known as *cyclostationarity*, describes signals whose statistical characteristics vary periodically over time [13]. Unfortunately, the aforementioned stationarities of graph signals, i.e., GWSS and JWSS, are limited to accommodate cyclostationarity, which negatively affects application performance. In other words, they may be improved if we can appropriately estimate period(s) from TVGSs.

In this paper, we propose a period estimation method for TVGSs based on the cyclostationarity assumption, and apply it to graph Wiener filter. First, we propose cyclic graph wide sense stationarity (CGWSS) for TVGSs. Second, we present a method to extract periodic features from TVGSs with the following two phases. In the first phase, we decompose a set of signals using two dictionaries: GFT [2] and a nested periodic dictionary (NPD) [14]. GFT captures spatial features, and NPD is designed to capture temporal fundamental periods with multiple discrete Fourier transform (DFT) matrices [14]. In the second phase, the dominant period of the TVGSs is identified from the features extracted in the first phase. The period estimation method is formulated as a convex optimization and is solved by iterative shrinkage thresholding algorithm (ISTA) [15]. Based on the estimated period and the CGWSS assumption, we derive cyclic graph Wiener filter (CGWF) for periodic TVGSs.

Numerical experiments with two real-world datasets demonstrate that the proposed method accurately estimates the period and the CGWF exhibits superior estimation performance to existing methods.

Notation: $[\mathbf{A}]_{m,n}$ denotes the (m,n)-element of $\mathbf{A}$. We use $[\mathbf{X}]_{m_1:m_2,n_1:n_2}$ to denote the submatrix of $\mathbf{X}$ whose rows are indexed from m_1 to m_2, and columns from n_1 to n_2. In particular, $[\mathbf{X}]_{m,:}$ denotes the m-th row vector of $\mathbf{X}$, and $[\mathbf{X}]_{:,n}$ denotes the n-th column vector. The vectorization operator is denoted by $\mathrm{vec}(\cdot)$. The symbol $\otimes$ represents Kronecker product and $\mathbf{x}^H$ indicates the Hermitian transpose of $\mathbf{x}$. The remainder of a modulo b is written $a \bmod b$, and the greatest common divisor of two integers a and b is denoted by $\gcd(a,b)$. Kronecker delta is defined as $\delta_{i,j} = 1$ if $i = j$ and 0 otherwise.

A weighted undirected graph is denoted by $\mathcal{G} = (\mathcal{V}, \mathcal{E})$, in which $\mathcal{V}$ and $\mathcal{E}$ are sets of nodes and edges, respectively. The number of nodes and edges are denoted by $N = |\mathcal{V}|$ and

979-8-3315-7206-8/25/$31.00

$E = |\mathcal{E}|$, respectively. We use a weighted adjacency matrix $\mathbf{W}$ for representing the connection between nodes, where its (m,n)-element $[\mathbf{W}]_{m,n} \geq 0$ is the edge weight between the mth and nth nodes; $[\mathbf{W}]_{m,n} = 0$ for unconnected nodes. The degree matrix $\mathbf{D}$ is a diagonal matrix whose each element is defined as $[\mathbf{D}]_{m,m} = \sum_n [\mathbf{W}]_{m,n}$. Using $\mathbf{D}$ and $\mathbf{W}$, the graph Laplacian is given by $\mathbf{L} = \mathbf{D} - \mathbf{W}$ [2]. A graph signal $\mathbf{x} \in \mathbb{R}^N$ is defined as $\mathbf{x} : \mathcal{V} \to \mathbb{R}^N$ where $[\mathbf{x}]_n$ corresponds to the signal value at the nth node. A TVGS at t time instance is expressed by $\mathbf{x}_t \in \mathbb{R}^N$ and TVGSs with the time length T are $\mathbf{X} = [\mathbf{x}_1, \ldots, \mathbf{x}_T] \in \mathbb{R}^{N \times T}$. Since $\mathbf{L}$ is a real symmetric matrix, it has orthogonal eigenvectors and can be diagonalized as $\mathbf{L} = \mathbf{U}\mathbf{\Lambda}\mathbf{U}^\top$, where $\mathbf{U} = [\mathbf{u}_0, \mathbf{u}_1, \ldots, \mathbf{u}_{N-1}]$ is a matrix whose ith column is the eigenvector $\mathbf{u}_i$ and $\mathbf{\Lambda} = \mathrm{diag}(\lambda_0, \lambda_1, \ldots, \lambda_{N-1})$ is their diagonal eigenvalue matrix. Without loss of generality, we can assume $0 = \lambda_0 \leq \lambda_1, \ldots, \lambda_{N-1} = \lambda_{\max}$ since $\mathbf{L}$ is a positive semidefinite matrix. In graph signal processing (GSP), λ_i is referred to as a *graph frequency* [2]. Then, spectra of $\mathbf{x}$ in the graph frequency domain are defined as $\hat{\mathbf{x}} = \mathbf{U}^\top \mathbf{x}$: It is called *graph Fourier transform* (GFT) [2].

II. Related Work

In this section, we first review WSS for standard time domain signals. Then, GWSS and JWSS for TVGSs are introduced as its counterparts for the graph setting.

A. Wide Sense Stationarity

WSS for standard time domain signals is defined as follows:

Definition 1 (WSS [16])**.** *A finite-length discrete time domain signal $\mathbf{v} = [v[1], \ldots, v[T]]^\top \in \mathbb{R}^T$ is a WSS process if and only if the following conditions are satisfied:*

$$\mathbb{E}[\mathbf{v}] = \boldsymbol{\mu}_v, \tag{1a}$$

$$\mathbb{E}\left[\mathbf{v}\mathbf{v}^\top\right] = \mathbf{\Gamma} = \mathbf{F}\mathrm{diag}(\mathbf{p}_v)\mathbf{F}^H, \tag{1b}$$

where $\boldsymbol{\mu}_v \in \mathbb{R}^T$, $\mathbf{\Gamma} \in \mathbb{R}^{T \times T}$, $\mathbf{F} \in \mathbb{C}^{T \times T}$, and $\mathbf{p}_v \in \mathbb{R}^T$ are the mean, auto-covariance matrix, discrete Fourier transform (DFT) matrix, and power spectral density (PSD), respectively.

One of the most important properties of WSS in Definition 1 is that the auto-covariance matrix $\mathbf{\Gamma}$ is diagonalized by the DFT matrix $\mathbf{F}$. This property follows from Wiener-Khinchin theorem [16].

Note that $\mathbf{\Gamma}$ in (1b) is a symmetric circular Toeplitz matrix, where its (m,n)-element depends solely on the time shift, i.e., $(m-n) \bmod T$. This implies that the Wiener-Khinchin property arises from the (circular) shift invariance of $\mathbf{\Gamma}$. Formally, it is translated into

$$\mathbf{S}\mathbf{\Gamma} = \mathbf{\Gamma}\mathbf{S}, \tag{2}$$

where $\mathbf{S} \in \mathbb{R}^{T \times T}$ is the cyclic shift operator in the discrete time domain with the period T, i.e., $[\mathbf{S}]_{m,n} = \delta_{m,(n+1) \bmod T}$.

B. Graph Wide Sense Stationarity

Suppose that a graph signal $\mathbf{x} \in \mathbb{R}^N$ is a random process in the node domain. GWSS for random graph signals is a natural extension of the above mentioned WSS. It is defined as follows:

Definition 2 (GWSS [3])**.** *The signal $\mathbf{x}$ follows a GWSS process if and only if the following conditions are satisfied:*

$$\mathbb{E}[\mathbf{x}] = \boldsymbol{\mu}_x, \tag{3a}$$

$$\mathbb{E}\left[\mathbf{x}\mathbf{x}^\top\right] = \mathbf{\Sigma} = \mathbf{U}\mathrm{diag}(\mathbf{p}_x)\mathbf{U}^\top, \tag{3b}$$

where $\boldsymbol{\mu}_x$, $\mathbf{\Sigma}$ and $\mathbf{p}_x$ are the mean, covariance matrix, and graph PSD, respectively.

In (3b), the covariance $\mathbf{\Sigma}$ is diagonalizable by $\mathbf{U}$, instead of $\mathbf{F}$ in Definition 1. This property parallels the Wiener-Khinchin relation in the time domain in (1b). Similar to (2), (3b) holds if and only if the following equality is satisfied [5]:

$$\mathbf{L}\mathbf{\Sigma} = \mathbf{\Sigma}\mathbf{L}. \tag{4}$$

We can view that (4) is the graph counterpart of (2), where $\mathbf{S}$ is replaced with $\mathbf{L}$, and $\mathbf{\Gamma}$ corresponds to $\mathbf{\Sigma}$.

C. Joint Wide Sense Stationarity

GWSS only assumes the spatial characteristics of a random graph signal $\mathbf{x}$. That is, it does not consider the temporal relationships of TVGSs. JWSS is an extension of GWSS for the time-varying scenario.

Suppose that TVGSs $\mathbf{X} \in \mathbb{R}^{N \times T}$ are a random process on both the node and time domains. JWSS assumes the stationarity of TVGSs in the *joint node-time domain*, where WSS in Definition 1 and GWSS in Definition 2 simultaneously hold [7].

Here, let $[\mathbf{\Gamma}]_{m,n} = \mathbb{E}[[\mathbf{X}]_{m,:}^\top [\mathbf{X}]_{n,:}] \in \mathbb{R}^{T \times T}$ be the covariance matrix between the nodes m and n. According to (2), the shift invariance in the time domain for TVGSs is given by $\mathbf{S}\mathbf{\Gamma}_{m,n} = \mathbf{\Gamma}_{m,n}\mathbf{S}$. By merging this with (4), JWSS relation is represented as

$$(\mathbf{S} \otimes \mathbf{L})\mathbf{\Sigma}_{\mathrm{J}} = \mathbf{\Sigma}_{\mathrm{J}}(\mathbf{S} \otimes \mathbf{L}), \tag{5}$$

where $\mathbf{\Sigma}_{\mathrm{J}}$ is given by

$$\mathbf{\Sigma}_{\mathrm{J}} = \begin{bmatrix} \mathbf{\Gamma}_{1,1} & \mathbf{\Gamma}_{1,2} & \cdots & \mathbf{\Gamma}_{1,N} \\ \mathbf{\Gamma}_{2,1} & \mathbf{\Gamma}_{2,2} & \cdots & \mathbf{\Gamma}_{2,N} \\ \vdots & \vdots & \ddots & \vdots \\ \mathbf{\Gamma}_{N,1} & \mathbf{\Gamma}_{N,2} & \cdots & \mathbf{\Gamma}_{N,N} \end{bmatrix}. \tag{6}$$

Followed by (5), $\mathbf{X}$ can be a JWSS process if $\mathbf{\Sigma}_J$ and $\mathbf{S} \otimes \mathbf{L}$ are jointly diagonalizable. However, if $\mathbf{X}$ exhibits cyclostationarity over the interval T, the submatrices $\mathbf{\Gamma}_{m,n}$ lose their symmetric circular Toeplitz structure and instead form block circulant matrices. Consequently, (5) no longer holds.

III. Preliminaries

In this section, we introduce several analysis techniques used in our method. First, we introduce the standard GWF based on the GWSS assumption [3]. Second, we review NPD [14].

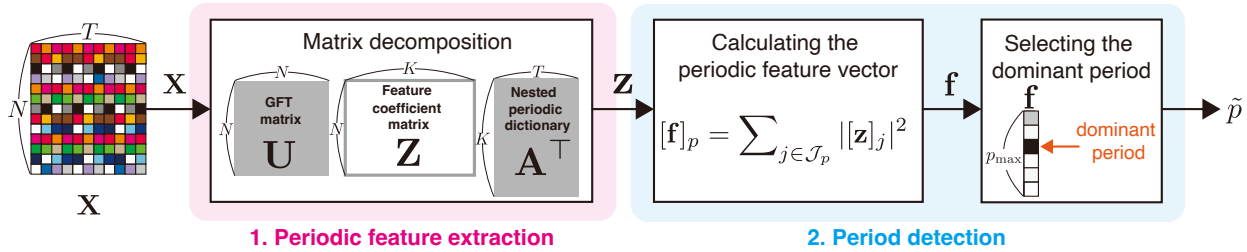

Fig. 1: Overview of the period estimation method for TVGSs.

A. Graph Wiener filter

Suppose that a random graph signal $\mathbf{x}$ is a GWSS process. We consider the following observation model:

$$\mathbf{y} = \mathbf{M}\mathbf{x} + \mathbf{n}, \quad \mathbf{n} \sim \mathcal{N}(\mathbf{0}, \sigma^2\mathbf{I}), \tag{7}$$

where $\mathbf{M} \in \mathbb{R}^{M\times N}$ $(M \leq N)$ is a measurement matrix and $\mathbf{n} \in \mathbb{R}^M$ is additive white Gaussian noise with the standard deviation σ.

Here, we would like to recover $\mathbf{x}$ from $\mathbf{y}$. The reconstructed signal $\tilde{\mathbf{x}}$ can be generally written as $\tilde{\mathbf{x}} = \mathbf{H}\mathbf{y} + \mathbf{b}$, where $\mathbf{H} \in \mathbb{R}^{N\times M}$ is a recovery filter and $\mathbf{b} \in \mathbb{R}^N$ is a bias component. One of the representative criteria for recovering random processes is the minimum mean squared error (MMSE) criterion. To determine the optimal $\mathbf{H}$ and $\mathbf{b}$, we formulate the following optimization problem based on the MMSE criterion [3]:

$$\underset{\{\mathbf{H},\mathbf{b}\}}{\operatorname{argmin}}\, \mathbb{E}[||\tilde{\mathbf{x}} - \mathbf{x}||_2^2]. \tag{8}$$

If $\mathbf{x}$ is a GWSS process in Definition 2, (8) can be analytically solved as:

$$\begin{aligned} \mathbf{H} &= \mathbf{\Sigma}\mathbf{M}^\top(\mathbf{M}\mathbf{\Sigma}\mathbf{M}^\top)^{-1}, \\ \mathbf{b} &= (\mathbf{I} - \mathbf{H}\mathbf{M})\boldsymbol{\mu}_x. \end{aligned} \tag{9}$$

The solution in (9) is referred to as GWF [3].

B. Nested Periodic Dictionary

NPD is a matrix constructed from DFT matrices with multiple fundamental periods. It is used for measuring temporal relationships of standard time domain signals with several periods [14].

Let $p_{\max} \in \mathbb{N}_+$ be the maximum period we would like to detect, and let $p \in \{1, \ldots, p_{\max}\}$ be a positive integer up to $p_{\max}$. For a time duration T, NPD $\mathbf{A} \in \mathbb{C}^{T\times K}$ is defined as [14]:

$$\mathbf{A} = \begin{bmatrix} \mathbf{D}_1 & \mathbf{D}_2 & \cdots & \mathbf{D}_{p_{\max}} \\ \mathbf{D}_1 & & & \\ \mathbf{D}_1 & \mathbf{D}_2 & & \\ \mathbf{D}_1 & & & \\ \vdots & \vdots & \ddots & \vdots \\ \widehat{\mathbf{D}}_1 & \widehat{\mathbf{D}}_2 & \cdots & \widehat{\mathbf{D}}_{p_{\max}} \end{bmatrix}, \tag{10}$$

where $\mathbf{D}_p \in \mathbb{C}^{p\times\phi(p)}$ is a submatrix of DFT[1] and $\widehat{\mathbf{D}}_p$ is the truncated version of $\mathbf{D}_p$ adjusted to match the row dimension of $\mathbf{A}$. Formally, $\mathbf{D}_p$ and $\widehat{\mathbf{D}}_p$ are represented as follows:

$$\mathbf{D}_p = \begin{bmatrix} W_p^{k_1\cdot 0} & W_p^{k_2\cdot 0} & \cdots & W_p^{k_{\max}\cdot 0} \\ W_p^{k_1\cdot 1} & W_p^{k_2\cdot 1} & \cdots & W_p^{k_{\max}\cdot 1} \\ \vdots & \vdots & \ddots & \vdots \\ W_p^{k_1\cdot p-1} & W_p^{k_2\cdot p-1} & \cdots & W_p^{k_{\max}\cdot p-1} \end{bmatrix}, \tag{11}$$

$$\widehat{\mathbf{D}}_p = [\mathbf{D}_p]_{1:p-T \bmod p,:},$$

where $W_p^{k_i\cdot d} = e^{-j2\pi\frac{k_i d}{p}}$ $(d \in \{0, 1, \ldots, p-1\})$ and k_i is an integer that satisfies $1 \leq k_i \leq p$ and $\gcd(k_i, p) = 1$[2].

Note that $\mathbf{D}_p$ is defined as the collection of p-point DFT bases corresponding to fundamental periods k_i that are coprime with p. Thus, $\mathbf{A}$ is designed to include bases for all candidate fundamental periods from 1 to $p_{\max}$.

IV. Period Estimation for TVGSs and Cyclic Graph Wiener Filter

In this section, we first propose CGWSS for TVGSs. Next, we propose a period estimation method and derive the CGWF based on CGWSS assumption.

A. Cyclic Graph Wide Sense Stationarity

To take into account the periodicity of TVGSs, we assume that a TVGS $\mathbf{x}_t$ satisfies the conditions defined below:

Definition 3 (CGWSS). *A TVGS $\mathbf{x}_t$ is a cyclic graph wide sense stationary process if and only if the following conditions are satisfied:*

$$\mathbb{E}[\mathbf{x}_{t \bmod p}] = \boldsymbol{\mu}_{t \bmod p}, \tag{12a}$$

$$\mathbb{E}\left[\mathbf{x}_{t \bmod p}\mathbf{x}_{t \bmod p}^\top\right] = \mathbf{\Sigma}_{t \bmod p} = \mathbf{U}\mathrm{diag}(\mathbf{p}_{t \bmod p})\mathbf{U}^\top, \tag{12b}$$

where p denotes the period of the TVGS, and $\boldsymbol{\mu}_{t \bmod p}$, $\mathbf{\Sigma}_{t \bmod p}$, and $\mathbf{p}_{t \bmod p}$ are the cyclic mean, covariance, and graph PSD, respectively.

CGWSS can be considered as a generalized version of GWSS [3] for TVGSs since CGWSS is identical to GWSS in Definition 2 when $p = 1$.

Note that CGWSS in Definition 3 requires the period p while we rarely know its exact value in practice. Next, we propose a period estimation method for TVGSs.

[1] $\phi(\cdot)$ is an Euler's totient function [17]. It is defined as $\phi(n) = \#\{k \in \mathbb{N}_+ | 1 \leq k \leq n, \gcd(k, n) = 1\}$.

[2] The sequence of k_i satisfies $1 = k_1 < k_2 < \cdots < k_{\phi(p)} = k_{\max}$.

B. Period Estimation for TVGSs

We estimate the period of TVGSs in two phases: 1) periodic feature extraction and 2) period detection. We illustrate its overview in Fig. 1. In the following, we describe the details of these two phases.

1) Periodic feature extraction: Let $\mathbf{X} = [\mathbf{x}_1, \dots, \mathbf{x}_T] \in \mathbb{R}^{N \times T}$ be a collection of TVGSs. First, we assume that $\mathbf{X}$ is approximately represented using GFT as a spatial dictionary and NPD as a temporal one, as follows:

$$\mathbf{X} \approx \mathbf{U}\mathbf{Z}\mathbf{A}^\top, \tag{13}$$

where $\mathbf{Z} \in \mathbb{C}^{N \times K}$ is the sparse feature coefficient matrix. Then, we estimate $\mathbf{Z}$ in (13) using a sparse coding technique. Similar to LASSO [15], we can formulate the problem as

$$\min_{\mathbf{z}} ||\mathbf{c} - \mathbf{T}\mathbf{z}||_2^2 + \eta ||\mathbf{z}||_1, \tag{14}$$

where $\mathbf{c} = \mathrm{vec}(\mathbf{X}) \in \mathbb{R}^{NT}$, $\mathbf{z} = \mathrm{vec}(\mathbf{Z}) \in \mathbb{C}^{NK}$, $\mathbf{T} = \mathbf{A} \otimes \mathbf{U} \in \mathbb{C}^{NT \times NK}$. In (14), the first term enforces the fidelity to the data $\mathbf{c}$, and the second term, weighted by the parameter η, facilitates the sparsity of $\mathbf{z}$. Since (14) is convex, it can be easily solved by applying ISTA [15]: Its algorithm is summarized in Algorithm 1. In Algorithm 1, we utilize the following operators:

- $\nabla f(\mathbf{z}) = \mathbf{T}^\top(\mathbf{T}\mathbf{z} - \mathbf{c})$,
- $[\mathrm{prox}_{\frac{\eta}{\rho}||\cdot||_1}(\mathbf{z})]_i = \mathrm{sgn}([\mathbf{z}]_i) \max(|[\mathbf{z}]_i| - \frac{\eta}{\rho}, 0)$.

Algorithm 1: ISTA for solving (14)

Input: $\mathbf{c}, \mathbf{T}, \eta, \rho, \epsilon$.
Initialization: $\mathbf{z}^{(0)} = \mathbf{0}$
for $t = 1, 2, \dots$ **do**
  $\mathbf{z}^{(t)} = \mathrm{prox}_{\frac{\eta}{\rho}\|\cdot\|_1}(\mathbf{z}^{(t-1)} - \frac{1}{\rho}\nabla f(\mathbf{z}^{(t-1)}))$
  if $||\mathbf{z}^{(t)} - \mathbf{z}^{(t-1)}||_2 < \epsilon$ **then**
    break
Output: $\mathbf{z} = \mathbf{z}^{(t)}$

2) Period detection: To determine the period of $\mathbf{X}$ from $\mathbf{z}$, we introduce the periodic feature vector $\mathbf{f} \in \mathbb{R}^{p_{\max}}$ as follows:

$$[\mathbf{f}]_p = \sum_{j \in \mathcal{J}_p} |[\mathbf{z}]_j|^2, \tag{15}$$

where $\mathcal{J}_p = \{j \,|\, j = n + (p-1)N, n = 1, \dots, N\}$ is a set of indices in $\mathbf{z}$ corresponding to the features extracted from submatrix $\mathbf{D}_p$ of the dictionary $\mathbf{A}$ (see (10) and (13)). Note that (15) groups the features in $\mathbf{z}$ according to their corresponding periods $p \in \{1, \dots, p_{\max}\}$. That is, the pth entry in $\mathbf{f}$ represents the aggregated energy of $\mathbf{z}$ associated with period p.

We estimate the period p by choosing $\mathrm{argmax}_p[\mathbf{f}]_p$, which corresponds to the dominant period.

TABLE I: Hyperparameter configuration for each dataset in the period estimation.

	Number of nodes N	Time length T	Maximum period in (10) $p_{\max}$	Hyperparameters used for ISTA		
				η	ρ	ϵ
SST	268	108	15	1.0	300	0.01
NYT	419	100	10	1.0	100	0.01

C. Cyclic Graph Wiener Filter

We derive a graph Wiener filter for periodic TVGSs. We assume that a TVGS $\mathbf{x}_t$ conforms to CGWSS in Definition 3 and consider the same observation model as (7). Our goal is to recover $\mathbf{x}_t$ from $\mathbf{y}_t$. In the same fashion as (8), we consider the optimization problem based on MMSE criterion as follows:

$$\underset{\{\mathbf{H}_t, \mathbf{b}_t\}}{\mathrm{argmin}}\, \mathbb{E}[||\tilde{\mathbf{x}}_t - \mathbf{x}_t||_2^2]. \tag{16}$$

Analogous to (9), (16) can be easily solved and the CGWF is derived as:

$$\begin{aligned} \mathbf{H}_{t \bmod p} &= \mathbf{\Sigma}_{t \bmod p}\mathbf{M}^\top(\mathbf{M}\mathbf{\Sigma}_{t \bmod p}\mathbf{M}^\top)^{-1}, \\ \mathbf{b}_{t \bmod p} &= (\mathbf{I} - \mathbf{H}_{t \bmod p}\mathbf{M})\boldsymbol{\mu}_{t \bmod p}. \end{aligned} \tag{17}$$

Thus, the reconstructed signal in (17) is given by $\tilde{\mathbf{x}}_{t \bmod p} = \mathbf{H}_{t \bmod p}\mathbf{y}_{t \bmod p} + \mathbf{b}_{t \bmod p}$.

Note that, when $p = 1$, the CGWF in (17) is reduced to the GWF in (9).

V. Experiments

In this section, we perform period estimation and signal reconstruction experiments on two real-world datasets.

A. Datasets

We use the following two datasets, whose characteristics are summarized in Table I:

Sea Surface Temperature (SST) [18]: It records snapshots of global SSTs (°C) for every month from 2004 to 2021 (216 months). Each SST is observed at intersections of 1-degree latitude-longitude grids. We randomly sample $N = 268$ intersections and they are regarded as nodes. Then, we construct a five-nearest neighbor graph using the sampled nodes, where the edge weights are assigned based on the Euclidean distance between the node coordinates [19].

New York City Subway Traffic (NYT) [20]: It records the number of passengers over $N = 419$ stations in New York City subway. The data are collected six times a day on weekdays with four-hour intervals from 2017 to 2021. We construct an unweighted undirected graph based on the adjacency relationships of actual railway routes. We extract 200 samples recorded from March 1st, 2018 to April 17th, 2018 and use them for the experiment.

B. Experimental Setup

Period Estimation: In the period estimation experiments, we use the first half of SST and NYT: The first 108 monthly snapshots (from Jan. 2004 to Dec. 2012) in SST, and 100

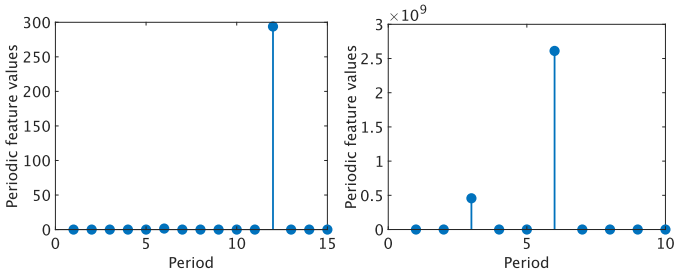

(a) SST (b) NYT

Fig. 2: Period estimation results under noise-free conditions.

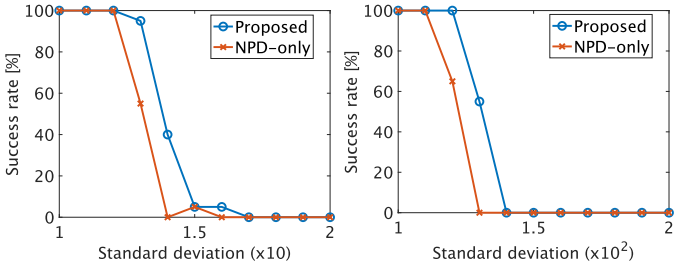

(a) SST (b) NYT

Fig. 3: Period estimation accuracies across different standard deviations σ of noise. The vertical axis shows the success rate.

samples (from Mar. 1st, 2018 to Mar. 23rd, 2018) in NYT. The configurations of hyperparameters are summarized in Table I.

We employ the model in (7) and set the observation matrix as $\mathbf{M} = \mathbf{I}$. In (10), we limit the search to periods up to $p_{\max} = 15$ and $p_{\max} = 10$ for SST and NYT, respectively. The period estimation accuracy is measured across different noise levels ($\sigma \geq 0$ in (7)). For each σ, we perform 20 independent runs and compute the success rate where the estimated period exactly matches the ground truth period. The ground truth periods are set to $p = 12$ for SST (yearly periodicity), and $p = 6$ for NYT (daily periodicity).

We compare the success rates of the proposed method with those of the conventional method that only uses NPD in (13) [14]. We abbreviate it as NPD-only.

Signal Reconstruction: In the signal reconstruction experiments, the first half of the samples in the both datasets are used for training, and the remaining half for the test. We use a random sampling matrix $\mathbf{M}$ in (7) with varying node sampling ratio M/N from 0.7 to 1.0 in increments of 0.01.

We perform CGWF in (17) using the cyclic covariance $\mathbf{\Sigma}_{t \bmod p}$ for each $t \bmod p$. These covariances are estimated from the training data using the method presented in [4], [19]. We evaluate the average mean squared error (MSE) of CGWF via the test data under different standard deviations σ.

C. Experimental Results

Period Estimation: The obtained periodic feature vectors $\mathbf{f}$ in (15) under noise-free conditions are visualized in Fig. 2. Fig. 3 also plots the period estimation accuracies across different noise levels.

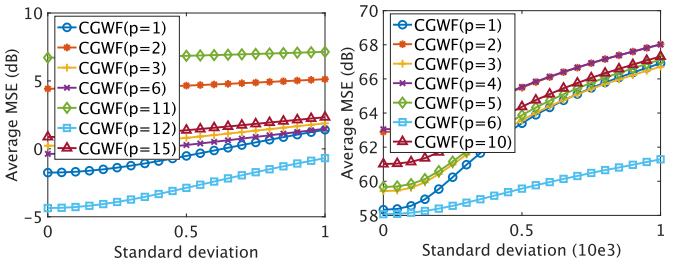

(a) SST (b) NYT

Fig. 4: Signal reconstruction results across different standard deviations σ with fixed node sampling ratio $M/N = 0.9$.

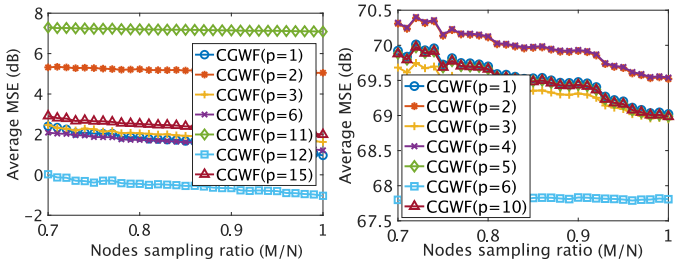

(a) SST (b) NYT

Fig. 5: Signal reconstruction results across different node sampling ratios M/N with fixed standard deviation $\sigma = 1$ for SST and $\sigma = 1 \times 10^3$ for NYT.

Figs. 2(a) and (b) show that the most significant periods of SST and NYT are $p = 12$ and $p = 6$, respectively. These results are reasonable in terms of the seasonal variations of SST and the transportation patterns of NYT. Even under noisy scenarios in Figs. 3(a) and (b), we observe that the proposed method maintains stable period estimation accuracy compared to the conventional NPD-only approach.

Signal Reconstruction: Figs. 4 and 5 illustrate the MSEs across different standard deviations and node sampling ratios. Figs. 6 and 7 also visualize examples of the absolute errors between the original and reconstructed signals.

From Figs. 4 and 5, we observe that the CGWF using the estimated periods, $p = 12$ in SST and $p = 6$ in NYT, are the most accurate for all period candidates. The CGWF also outperforms the standard GWF, i.e., CGWF with $p = 1$, which can also be observed from the visualizations in Figs. 6 and 7. This implies the importance of accurate period estimation for TVGSs in an application to graph Wiener filtering.

VI. Conclusion

In this paper, we propose a period estimation method for TVGSs and apply it to graph Wiener filter. Initially, we assume CGWSS on TVGSs in order to characterize the periodic stationarity of TVGSs. We propose a period estimation composed of two phases: in the first phase, we extract periodic features from TVGSs by decomposing a set of TVGSs using graph Fourier transform and a nested periodic dictionary; in the

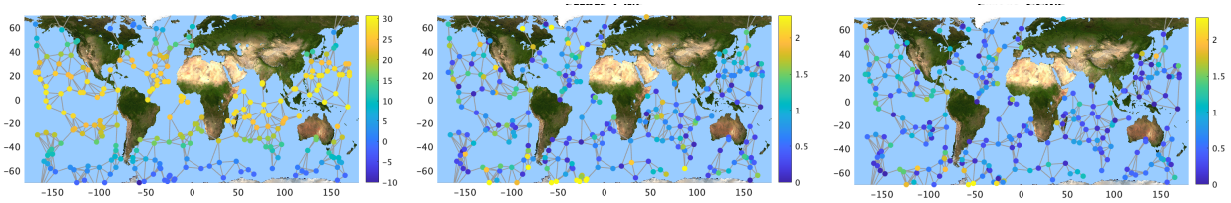

(a) Original (b) CGWF with $p = 1$ (GWF) (c) CGWF with $p = 12$

Fig. 6: Signal reconstruction experiments on SST. The color of a node indicates the absolute error between the original and reconstructed signal in (b) and (c).

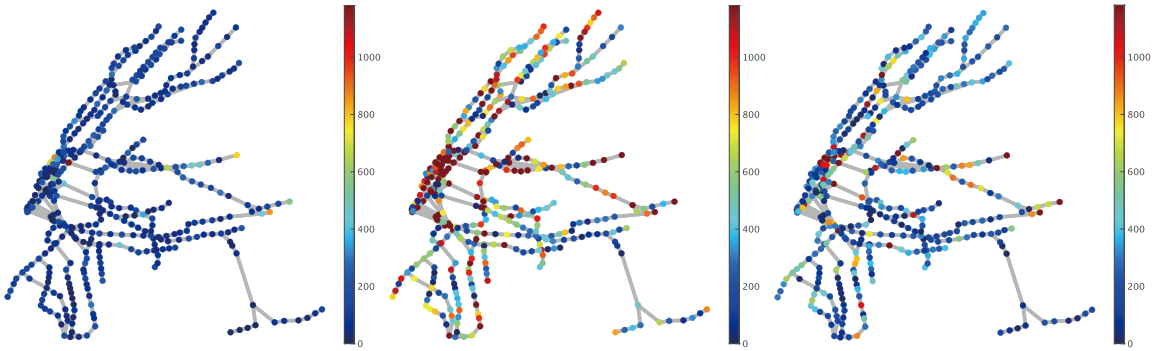

(a) Original (b) CGWF with $p = 1$ (GWF) (c) CGWF with $p = 6$

Fig. 7: Signal reconstruction experiments on NYT. The color of a node indicates the absolute error between the original and reconstructed signal in (b) and (c).

second phase, we obtain features that indicate the dominant period of TVGSs from the features extracted in the first phase. Finally, we derive CGWF based on the estimated period and CGWSS assumption. The period estimation and signal reconstruction experiments on real-world datasets demonstrate that our method effectively estimates the period of TVGSs.

REFERENCES

[1] I. F. Akyildiz, W. Su, Y. Sankarasubramaniam, and E. Cayirci, "A survey on sensor networks," *IEEE Commun. Mag.*, vol. 40, no. 8, pp. 102–114, 2002.

[2] D. I. Shuman, S. K. Narang, P. Frossard, A. Ortega, and P. Vandergheynst, "The emerging field of signal processing on graphs: Extending high-dimensional data analysis to networks and other irregular domains," *IEEE Signal Process. Mag.*, vol. 30, no. 3, pp. 83–98, 2013.

[3] N. Perraudin and P. Vandergheynst, "Stationary signal processing on graphs," *IEEE Trans. Signal Process.*, vol. 65, no. 13, pp. 3462–3477, 2017.

[4] A. G. Marques, S. Segarra, G. Leus, and A. Ribeiro, "Stationary graph processes and spectral estimation," *IEEE Trans. Signal Process.*, vol. 65, no. 22, pp. 5911–5926, 2017.

[5] J. Hara, Y. Tanaka, and Y. C. Eldar, "Graph signal sampling under stochastic priors," *IEEE Trans. Signal Process.*, vol. 71, pp. 1421–1434, 2023.

[6] S. K. Narang, Y.-H. Chao, and A. Ortega, "Critically sampled graph-based wavelet transforms for image coding," in *2013 Asia-Pac. Signal Inf. Process. Assoc. Annu. Summit Conf. (APSIPA)*, pp. 1–4, IEEE, 2013.

[7] N. Perraudin, A. Loukas, F. Grassi, and P. Vandergheynst, "Towards stationary time-vertex signal processing," in *Proc. IEEE ICASSP*, pp. 3914–3918, IEEE, 2017.

[8] F. Grassi, A. Loukas, N. Perraudin, and B. Ricaud, "A time-vertex signal processing framework: Scalable processing and meaningful representations for time-series on graphs," *IEEE Trans. Signal Process.*, vol. 66, no. 3, pp. 817–829, 2017.

[9] X. Jian and W. P. Tay, "Wide-sense stationarity in generalized graph signal processing," *IEEE Trans. Signal Process.*, vol. 70, pp. 3414–3428, 2022.

[10] N. Koenig-Lewis and E. E. Bischoff, "Seasonality research: The state of the art," *Int. J. Tour. Res.*, vol. 7, no. 4-5, pp. 201–219, 2005.

[11] A. Dai, "Recent climatology, variability, and trends in global surface humidity," *J. Clim.*, vol. 19, no. 15, pp. 3589–3606, 2006.

[12] B. L. Smith and M. J. Demetsky, "Traffic flow forecasting: comparison of modeling approaches," *J. Transp. Eng.*, vol. 123, no. 4, pp. 261–266, 1997.

[13] W. A. Gardner, A. Napolitano, and L. Paura, "Cyclostationarity: Half a century of research," *Signal Process.*, vol. 86, no. 4, pp. 639–697, 2006.

[14] S. V. Tenneti and P. Vaidyanathan, "Nested periodic matrices and dictionaries: New signal representations for period estimation," *IEEE Trans. Signal Process.*, vol. 63, no. 14, pp. 3736–3750, 2015.

[15] S. Boyd and L. Vandenberghe, *Convex optimization*. Cambridge University Press, 2004.

[16] N. Wiener, "Generalized harmonic analysis," *Acta mathematica*, vol. 55, no. 1, pp. 117–258, 1930.

[17] B. Kaliski, "Euler's totient function," in *Encyclopedia of Cryptography, Security and Privacy*, pp. 834–835, Springer, 2025.

[18] N. A. A. Rayner, D. E. Parker, E. B. Horton, C. K. Folland, L. V. Alexander, D. P. Rowell, E. C. Kent, and A. Kaplan, "Global analyses of sea surface temperature, sea ice, and night marine air temperature since the late nineteenth century," *J. Geophys. Res. Atmos.*, vol. 108, no. D14, 2003.

[19] N. Perraudin, J. Paratte, D. Shuman, L. Martin, V. Kalofolias, P. Vandergheynst, and D. K. Hammond, "Gspbox: A toolbox for signal processing on graphs," *arXiv preprint arXiv:1408.5781*, 2014.

[20] E. Deng, "Normal and new normal: Nyc subway traffic 2017-21." Available: https://www.kaggle.com/datasets/eddeng/nyc-subway-traffic-data-20172021, 2021. Accessed: Feb. 10, 2025.